Ab initio molecular dynamics simulation of liquid water by quantum Monte Carlo

Andrea Zen, Ye Luo, Guglielmo Mazzola, Leonardo Guidoni, and Sandro Sorella

---

Articles you may be interested in

Ab initio molecular dynamics with noisy forces: Validating the quantum Monte Carlo approach with benchmark calculations of molecular vibrational properties
J. Chem. Phys. **141**, 194112 (2014); 10.1063/1.4901430

On the room-temperature phase diagram of high pressure hydrogen: An ab initio molecular dynamics perspective and a diffusion Monte Carlo study
J. Chem. Phys. **141**, 024501 (2014); 10.1063/1.4886075

Molecular packing and chemical association in liquid water simulated using ab initio hybrid Monte Carlo and different exchange-correlation functionals
J. Chem. Phys. **132**, 204509 (2010); 10.1063/1.3437061

Benchmark all-electron ab initio quantum Monte Carlo calculations for small molecules
J. Chem. Phys. **132**, 034111 (2010); 10.1063/1.3288054

The influence of temperature and density functional models in ab initio molecular dynamics simulation of liquid water
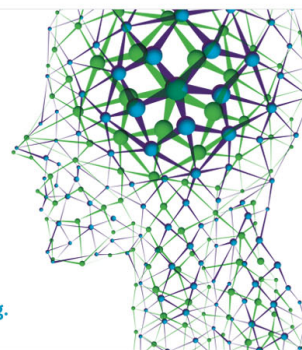J. Chem. Phys. **122**, 014515 (2005); 10.1063/1.1828433

Ab initio molecular dynamics simulation of liquid water by quantum Monte Carlo

Andrea Zen,[1,2,a)] Ye Luo,[3,4,b)] Guglielmo Mazzola,[3,4,c)] Leonardo Guidoni,[1,5,d)] and Sandro Sorella[3,4,e)]

[1]*Dipartimento di Fisica, "La Sapienza" - Università di Roma, piazzale Aldo Moro 5, 00185 Rome, Italy*
[2]*London Centre for Nanotechnology, University College London, London WC1E 6BT, United Kingdom*
[3]*SISSA–International School for Advanced Studies, Via Bonomea 26, 34136 Trieste, Italy*
[4]*Democritos Simulation Center CNR–IOM Istituto Officina dei Materiali, 34151 Trieste, Italy*
[5]*Dipartimento di Scienze Fisiche e Chimiche, Università degli Studi dell' Aquila, via Vetoio, 67100 L' Aquila, Italy*

Although liquid water is ubiquitous in chemical reactions at roots of life and climate on the earth, the prediction of its properties by high-level *ab initio* molecular dynamics simulations still represents a formidable task for quantum chemistry. In this article, we present a room temperature simulation of liquid water based on the potential energy surface obtained by a many-body wave function through quantum Monte Carlo (QMC) methods. The simulated properties are in good agreement with recent neutron scattering and X-ray experiments, particularly concerning the position of the oxygen-oxygen peak in the radial distribution function, at variance of previous density functional theory attempts. Given the excellent performances of QMC on large scale supercomputers, this work opens new perspectives for predictive and reliable *ab initio* simulations of complex chemical systems. © 2015 AIP Publishing LLC. [http://dx.doi.org/10.1063/1.4917171]

I. INTRODUCTION

The simulation by first principles of liquid water, the key element of human life and biological processes, has been a dream for several decades after the foundation of Density Functional theory (DFT), even within the restriction of the Born-Oppenheimer approximation for the heavy nuclei. Realistic simulations are particularly important because, at the experimental level, it is not possible to clarify completely what are the relationships between the so many different and rich phases of water and the physical interactions between water molecules, determined by hydrogen bonding and weak long-range van der Waals (vdW) interactions. Moreover, water is involved in many biological and chemical processes, and first principle simulations are useful to investigate and rationalize such important mechanisms.

The first attempted simulations date back to the pioneer works by Car and Parrinello,[1–3] within an efficient *ab initio* molecular dynamics (AIMD) based on DFT. The comparison with the experiments, at that time available, provided a pretty good agreement with the oxygen-oxygen (O–O) radial distribution function (RDF), as far as the positions of the peaks were concerned, but the overall shape given by the simulation was overstructured. After these first studies, many other works reporting standard DFT-based simulations have been published, but the agreement with the experimental data is still not satisfactory on many aspects. The equilibrium density at ambient pressure (1 atm $\sim 10^{-4}$ GPa) is far to be consistent with the expected one (1 gr/cm^3) though recent DFT functionals including van der Waals substantially reduce this discrepancy.[4] The simulated diffusion[5] is much lower than what is expected from experiments,[6] and, at least in some functionals (namely, PBE and BLYP), the solidification of water occurs at a temperature which is unrealistically large (~ 410 K), so that some of the present DFT simulations of liquid water should be considered supercooled metastable phases.[6,7]

The DFT results (about which we provide a brief summary in Table I) appear to be substantially influenced not only by the choice of the functional,[5,8] but also, within a given functional, by other details of the electronic calculations such as the pseudo-potential[6] and the basis set[9,10] (even though all these sources of errors are perfectly controllable, including the size effects[5,11] and the choice of the fictitious mass in the Car-Parrinello AIMD (CPMD),[11,12] at the cost of increasing the computational cost of the simulations). The mostly used functionals for liquid water are those based on the generalized gradient approximation (GGA) to DFT (often PBE or BLYP density functionals), yielding an overstructured water at ambient conditions. The accurate description of the exchange term by using the computationally more-expensive hybrid functionals was shown to improve significantly the results,[13–16] although they are still far from the experimental observation probably due to their poor description of the long-range interaction forces. On the other hand, in order to overcome the well-known difficulty of DFT in describing long range interaction forces, the inclusion of empirical dispersion terms has been attempted either by using empirical pairwise interatomic potentials (of the $C_6 R^{-6}$ form) in the total energy[17,18] or by adopting dispersion-corrected atom-centered

a)a.zen@ucl.ac.uk
b)xw111luoye@gmail.com
c)gmazzola@phys.ethz.ch
d)leonardo.guidoni@univaq.it
e)sorella@sissa.it

TABLE I. Structural properties (position and height of the nearest neighbor maximum in $g_{OO}(r)$ and minimum) and computational details for several *ab initio* simulations of liquid water in ambient conditions, as reported in recent literature for DFT-based molecular dynamics with PBE or BLYP functionals, in comparison with experiments and VMC-based results obtained in this work. The dynamics column indicates if results are obtained using Born-Oppenheimer (BO) molecular dynamics, Car-Parrinello (CP) molecular dynamics, second generation Car-Parrinello (2GCP) molecular dynamics,[48] Monte Carlo (MC) sampling, or the Langevin dynamics (LD) adopted in this work. The number in the parenthesis in the CP dynamics identifies the value of the fictitious mass of the electron μ. The sampling time corresponds to the production run.

References	N	System	Method	Dynamics	Ensemble	Sampling	T_{ion} (K)	r_{MAX}	g_{MAX}	r_{min}	g_{min}
Grossman *et al.*[11]	32	H_2O	BLYP	CP(340)	NVE	20 ps	285.9	2.73	3.65	3.32	0.40
Grossman *et al.*[11]	32	D_2O	BLYP	CP(340)	NVE	20 ps	297.5	2.73	3.60	3.33	0.39
Kuo *et al.*[12,a]	64	H_2O	BLYP	CP(400)	NVE	20 ps	314	2.76	2.90		
Kuo *et al.*[12,b]	64	H_2O	BLYP	BO	NVE	10 ps	323	2.76	3.00		
Kuo *et al.*[12,c]	64	H_2O	BLYP	MC	NVT		300	2.76	2.95		
Lee and Tuckerman[9]	32	D_2O	BLYP	CP(500)	NVT	30 ps	300	2.77	2.90		
Kühne *et al.*[5]	64	H_2O	BLYP	2GCP	NVT	30 ps	300	2.79	2.92	3.33	0.57
Lin *et al.*[23]	64	D_2O	BLYP	CP(600)	NVE	40 ps	319	2.77	2.86	3.31	0.66
Grossman *et al.*[11]	32	H_2O	PBE	CP(340)	NVE	20 ps	290.8	2.71	3.46	3.30	0.41
Grossman *et al.*[11]	54	H_2O	PBE	CP(340)	NVE	12 ps	298	2.73	3.75	3.36	0.78
Schwegler *et al.*[49]	54	H_2O	PBE	CP(340)	NVE	19.8 ps	296	2.69	3.65	3.32	0.37
Schwegler *et al.*[49]	54	H_2O	PBE	BO	NVE	20.5 ps	306	2.72	3.83	3.25	0.33
Kühne *et al.*[5]	64	H_2O	PBE	2GCP	NVT	250 ps	300	2.73	3.25	3.28	0.44
Lin *et al.*[23]	64	D_2O	PBE	CP(600)	NVE	40 ps	314	2.72	3.19	3.27	0.43
DiStasio *et al.*[16]	64	D_2O	PBE	CP(300)	NVT	>20 ps	300	2.69	3.28	3.28	0.37
DiStasio *et al.*[16]	64	D_2O	PBE0	CP(300)	NVT	>20 ps	300	2.71	2.96	3.30	0.53
DiStasio *et al.*[16]	64	D_2O	PBE+vdW	CP(300)	NVT	>20 ps	300	2.71	2.99	3.27	0.54
DiStasio *et al.*[16]	64	D_2O	PBE0+vdW	CP(300)	NVT	>20 ps	300	2.72	2.76	3.31	0.70
DiStasio *et al.*[16]	128	D_2O	PBE0+vdW	CP(300)	NVT	>20 ps	330	2.74	2.51	3.33	0.84
This work	32		VMC	LD	NVT		300	2.80	3.36	3.32	0.69
Experiment: Soper[34] (2013)							298	2.79	2.49		
Experiment: Skinner *et al.*[33] (2013)							298	2.80(1)	2.57(5)	3.45(4)	0.84(2)

[a]Simulation: CPMD-NVE-400.
[b]Simulation: CPMD-NVE-BO.
[c]Average of CP2K-MC-NVT-1 and CP2K-MC-NVT-2.

potentials.[19] Another possibility is the use of the van der Waals density functionals of Dion *et al.*[20] and further derivation based on nonlocal exchange-correlation functionals. All these approaches have provided remarkable improvements in some cases,[16,21–25] although these methods depend on external tunable parameters, and are strongly dependent on the functional. Recently, Morales *et al.*[26] have investigated the performances of several different DFT functionals versus very accurate diffusion Monte Carlo calculations, showing that the non-hybrid density functionals offer a poor description of the intramolecular potential energy surface, implying that there is still room for improvement of DFT functionals. Finally, quantum effects have been shown to have an important role, as they lead to a more accurate description of the hydrogen-bond, improving the agreement with experimental data[27–32] by broadening the RDF. Most of these achievements are very promising, as for instance the one reported in a recent paper by DiStasio *et al.*,[16] in which it is shown that the use of hybrid functionals, the inclusion of vdW/dispersion interactions, and the increase of the simulation temperature by 30 K determine a remarkably improved oxygen-oxygen radial distribution function. Anyway, the issue of the choice of the DFT functional still remains controversial, because it is not clear if, and to which extent, a better agreement with experiments corresponds

to a better description of the chemical and physical interactions between water molecules.

A recent accurate experiment of X-ray diffraction[33] has raised again the reliability issue of present *ab initio* molecular dynamics schemes, as it was found that, surprisingly, the position of the first peak was shifted towards larger distances. This observation is in excellent agreement with a recent extensive and independent review on the experimental structure of bulk water.[34] Indeed, in Ref. 34, a new methodology to interpret the experimental data is employed, and also, shifts of the intermolecular O–O, O–H and H–H peak positions with respect to the old experimental references[35] are reported, see Table I. These results are particularly important for *ab initio* simulations because the use of the PBE functional—until recently one of the most popular in this field—is being now replaced in favor of different functionals, like BLYP or B3LYP, that look clearly closer to present experiments.[5] In other words, we believe that, in order to make some progress for clarifying the present discrepancies between experiments and numerical simulations in this field, it is now timely to use a completely different approach for the following reasons:

- One of the main difficulties of DFT—within its current implementation with approximate functionals—is the

lack of a systematic way of improving the quality of the approximations employed, also because they cannot be validated by a variational principle as in wave function based approaches. Different functionals might be more suitable to tackle different problems, and in many cases, it is difficult to judge whether one functional is more accurate than another one for a given property without knowing the experimental result. This means that DFT requires alternative methods, able to validate new promising functionals, in order to establish properties of materials in special conditions to which experiments are not accessible, for instance, at very high pressures.

- The computing performances, especially in massively parallel architectures, are constantly growing with an impressive speed, as an exascale supercomputer is expected much before 2020, and supercomputer architectures are becoming more and more suitable for statistical techniques rather than for deterministic methods such as DFT. On such high performance computing machines, a wave function approach based on quantum Monte Carlo (QMC) is currently becoming practical and competitive with DFT, allowing to treat geometry optimization of molecules up to 100 atoms,[36] vibrational properties[37,38] and molecular dynamics simulations.[39,40]

Quantum Monte Carlo is a highly accurate wave function-based approach for electronic structure calculations[41] that has been also recently extended for *ab initio* simulations.[39,40,42–46] In this work, we have employed the first *ab initio* molecular dynamics simulation of liquid water based entirely on QMC. We adopt the Born-Oppenheimer approximation, neglecting the quantum effects on ions, and apply the variational Monte Carlo (VMC) approach using as an ansatz a Jastrow Slater many-body wave function. Even though we have used the simplest QMC approach, a significant improvement in the description of liquid water has been achieved. In particular, we have obtained that the O–O RDF, $g_{OO}(r)$, is considerably less structured compared with DFT calculations of the same type (with no proton quantum effects). Moreover, it is also worth to emphasize that the position of the first peak is now in perfect agreement with the most recent and accurate experiments, a fact that was, indeed, found with a simulation dated before the new experimental data were distributed.[47]

The paper is organized as follows: in Sec. II, we describe the methodological aspects of the QMC-based molecular dynamics simulation, and we provide the details about the variational ansatz used for the dynamics and its expected accuracy; in Sec. III, we discuss the results obtained simulating the liquid water by the QMC-based molecular dynamics (MD); and in Sec. IV, we discuss these results and draw the concluding remarks.

II. METHODOLOGICAL ASPECTS OF THE QMC-BASED MOLECULAR DYNAMICS

The molecular dynamics, driven by quantum Monte Carlo forces, was introduced recently for the simulation of liquid hydrogen at high pressures[39,40] and to obtain vibrational properties of molecular systems.[38] At fixed ion coordinates **R**, the

many-body wave function depends on the $N-$ electronic positions $x = \{\vec{r}_1, \vec{r}_2, \ldots, \vec{r}_N\}$ by means of the following Jastrow Slater (JSD) ansatz:

$$\Psi_{JSD} = J * \Psi_{SD}, \tag{1}$$

where Ψ_{SD} is a single Slater determinant and $J = e^U$ is the Jastrow factor. The Jastrow factor is a symmetric positive function of the electronic positions that depends on the inter-particle distances and describes the dynamical correlation among electrons. It is also particularly useful because, already in its simplest form, makes it possible to fulfill the electron-electron and electron-nucleus cusp conditions.[41,50,51] So far, the JSD ansatz can be efficiently simulated within a quantum Monte Carlo[41,51] approach that introduces no other bias than the statistical error, systematically vanishing with the simulation length.

An extensive discussion about the Langevin dynamics that we have used to integrate the equations of motions, when dealing with error affected nuclear force evaluations (because coming from QMC methods), has been already provided in Ref. 38, and the interested reader can refer to that. In the following, we instead want to discuss in much more details the variational ansatz that we have used for the specific system here under consideration. The choice of the ansatz (such as the functional form of the Jastrow and the basis set used) is of major importance in order to have accurate results within QMC calculations, as well as for any other wave function-based method. Thus, in Subsections II A and II B, we provide all the details concerning, respectively, the determinantal and Jastrow part of the wave function used in the VMC-based molecular dynamics. This wave function is the result of an extensive work for having a wave function that is accurate enough to provide reliable VMC results, and that is sufficiently compact (namely, that has a reasonably small number of parameters) that it can be stably and efficiently optimized in any MD step.

In order to show the quality of our approach, we have considered the water dimer, the simplest system in which the hydrogen bond is present, for which we report and compare, in Subsection II C, a number of tests of different basis sets and ansatzes, both at the variational and the fixed-node lattice regularized diffusion Monte Carlo scheme[52,53] (LRDMC). The latter method projects our approximate wave function to the exact ground state, with the approximation that the nodes of the wave function are pinned to the initial value determined by our ansatz. Among several advantages, LRDMC guarantees the full variational upper bound property of the energy, even when pseudo-potentials are used.[52,53]

Finally, the motivations for our final choice of the ansatz and basis set are reported in Subsection II D.

A. Determinant part Ψ_{SD} and its basis set

In the Slater determinant Ψ_{SD}, the double occupied molecular orbitals Ψ_i, with index $i = 1, \ldots, N/2$ (N is the number of electrons), are a linear combination of the localized atomic hybrid orbitals,[51]

$$\Psi_i(\mathbf{r}) = \sum_{a=1}^{M} \sum_{\mu_a=1}^{L_a} c_i^{a,\mu_a} \Phi_{a,\mu_a}(\mathbf{r}), \tag{2}$$

where Φ_{a,μ_a} is the μ_a-th atomic hybrid orbital of atom a, centered around the position $\mathbf{R}_a$ of nucleus a, M is the total number of atoms, L_a is the number of atomic hybrid orbitals used for atom a, for a total of $L = \sum_a L_a$ hybrid orbitals in the overall system, and the $M \times L$ coefficients c_i^{a,μ_a} are variationally optimized. The optimization is performed by using the correspondence between the single Slater determinant written in terms of molecular orbitals, and a truncated antisymmetrized geminal power (AGPn)[51,54] with $n = N/2$, with a geminal

$$g(\mathbf{r}_1, \mathbf{r}_2) = \sum_{a,b}^{M} \sum_{\mu_a}^{L_a} \sum_{\mu_b}^{L_b} g_{\mu_a,\mu_b}^{a,b} \Phi_{a,\mu_a}(\mathbf{r}_1) \Phi_{b,\mu_b}(\mathbf{r}_2), \quad (3)$$

those $L \times L$ parameters $g_{\mu_a,\mu_b}^{a,b}$ are related to c_i^{a,μ_a} by the relation

$$g_{\mu_a,\mu_b}^{a,b} = \sum_{i=1}^{N/2} c_i^{a,\mu_a} c_i^{b,\mu_b}. \quad (4)$$

The present formulation is adopted in the *TurboRVB* code,[55] because in this way, it is much simpler to satisfy symmetry properties (e.g., a spin singlet implies that the matrix g is symmetric) and to decrease the number of parameters by disregarding, during the optimization, those matrix elements, corresponding to atomic centers located at large distance each other (see later). Therefore, the parameters actually optimized in this approach are the $g_{\mu_a,\mu_b}^{a,b}$. They are then used to obtain the molecular orbital coefficients c_i^{a,μ_a} via the diagonalization described in Refs. 51 and 54. This choice gives a very important technical advantage for systems of large sizes as the one considered in this work. In particular, in order to decrease the total number of variational parameters, we have fixed to zero all the coefficients $g_{\mu_a,\mu_b}^{a,b}$ connecting the atoms a and b that are at a distance $R_{ab} = \|\mathbf{R}_a - \mathbf{R}_b\|$ larger than an appropriately chosen cutoff R_{MAX}. We will see in Secs. II B–II D that this choice does not significantly affect the accuracy of the calculation, but it is important because a much smaller number of variational parameters guarantees a stable and efficient wave function optimization.

The μ_a-th atomic hybrid orbital Φ_{a,μ_a} of the atom a is expressed as a linear combination of all the uncontracted orbitals $\phi_{a,l,k}$ introduced to describe the system

$$\Phi_{a,\mu_a}(\mathbf{r}) = \sum_{l=0}^{l_M(a)} \sum_{m=-l}^{+l} \sum_{k=1}^{K_M(a,l)} h_{a,l,m,k}\, \phi_{a,l,k}(r)\, Z_{l,m}(\Omega), \quad (5)$$

where l is the azimuthal quantum number, running from zero to the maximum angular momentum $l_M(a)$ of atom a; m is the magnetic quantum number; k labels the $K_M(a,l)$ orbitals of angular momentum l of the atom a in the chosen basis set; $Z_{l,m}(\Omega)$ is the real spherical harmonic; and $r = \|\mathbf{r}\|$ is the distance of the electron from the nucleus a. The coefficients $h_{a,l,m,k}$ are parameters that are variationally optimized.

The uncontracted orbitals implemented in *TurboRVB* code[55] are essentially Gaussian type orbital (GTO) or Slater type orbital (STO), with some possible modifications (as in the case of the STO s-orbital, modified in a way to avoid the electron-nucleus cusp, already satisfied by the chosen Jastrow factor) or generalizations (as for the case of the $r^2 * $ GTO s-orbital), allowing an improved description of the orbital

shape with the minimum possible number of variational parameters. In this work, the orbital functions that we have used are the following (for open systems):

- **s**-orbitals (*i.e.*, $l = 0$):

$$\phi_{\mathbf{s}}^{\mathrm{STO}}(r) \propto (1 + \zeta r)e^{-\zeta r}, \quad (6)$$

$$\phi_{\mathbf{s}}^{\mathrm{GTO}}(r) \propto e^{-\zeta r^2}, \quad (7)$$

$$\phi_{\mathbf{s}}^{r^2 * \mathrm{GTO}}(r) \propto r^2 e^{-\zeta r^2}, \quad (8)$$

- **p**-orbitals (*i.e.*, $l = 1$):

$$\phi_{\mathbf{p}}^{\mathrm{STO}}(r) \propto r e^{-\zeta r}, \quad (9)$$

$$\phi_{\mathbf{p}}^{\mathrm{GTO}}(r) \propto r e^{-\zeta r^2}, \quad (10)$$

- **d**-orbitals (*i.e.*, $l = 2$):

$$\phi_{\mathbf{d}}^{\mathrm{STO}}(r) \propto r^2 e^{-\zeta r}, \quad (11)$$

$$\phi_{\mathbf{d}}^{\mathrm{GTO}}(r) \propto r^2 e^{-\zeta r^2}. \quad (12)$$

whereas for systems with periodic boundary conditions (PBCs), as described in Refs. 56 and 57 and already used in Refs. 39, 43, and 57, the orbital functions are slightly modified, namely, the Cartesian distance $\mathbf{r}$ is replaced by a simple periodic function $\tilde{\mathbf{r}}(\mathbf{r})$ that takes into account the appropriate periodicity of the box. By consequence, also the distances $r = \|\mathbf{r}\|$ are replaced by new distances $\tilde{r} = \|\tilde{\mathbf{r}}\|$ and the normalization coefficients are correspondingly changed. In particular, we have used, here, the following substitution rule to modify an orbital used for open systems to PBC with box of lengths (L_x, L_y, L_z):

$$(x, y, z) \rightarrow (\tilde{x}, \tilde{y}, \tilde{z}) = \left(\frac{L_x}{\pi} \sin \frac{\pi x}{L_x}, \frac{L_y}{\pi} \sin \frac{\pi y}{L_y}, \frac{L_z}{\pi} \sin \frac{\pi z}{L_z} \right). \quad (13)$$

Other parametric forms for the atomic orbitals exist, see for instance Petruzielo *et al.*,[58] but are not used in this work. Each of the uncontracted orbitals described above depends parametrically only on the value of the ζ in the exponent that can be optimized as all the other variational parameters within our VMC calculations, see Refs. 51 and 59. In order to enhance the stability of the wave function optimization during the dynamics and to reduce the computational effort, we have optimized the values of the ζ exponents for the water dimer, namely, the smallest system with an hydrogen bond, and we have kept these exponents fixed in the VMC-based molecular dynamics.

The atomic basis set used in this work, including the orbital types and the exponent values for the oxygen and the hydrogen atoms, is specified in Table II.

B. Jastrow factor and its basis set

In the VMC-based molecular dynamics, we used the Jastrow factor

$$J = \exp(U_{en} + U_{ee} + U_{een})$$

that involves the one-electron interaction term U_{en}, the homogeneous two electron interaction term U_{ee}, and the inhomogeneous two-electron interaction term U_{een}, representing an

TABLE II. Basis set parameters in the wave function used for the VMC-based molecular dynamics. The two core electrons of the oxygen atoms have been described using the scalar-relativistic energy consistent pseudopotential of Burkatzki *et al.*[61]

Determinant part			
$R_{MAX} = 4.5$			
O: (5s,5p,1d)/{5}		H: (3s,1p)/{3}	
Type	ζ	Type	ζ
s-STO	2.037	s-STO	1.572
s-r^2* GTO	1.128	s-GTO	0.086
s-GTO	0.214	s-GTO	2.176
s-GTO	0.736		
s-GTO	3.617		
p-STO	1.199	p-STO	1.112
p-GTO	0.433		
p-GTO	1.408		
p-GTO	4.183		
p-GTO	10.380		
d-STO	1.202		
Jastrow part			
O: (3s,2p)		H: (2s,2p)	
type	ζ	type	ζ
s-G	2.022	s-G	1.648
s-G	0.507	s-G	0.051
s-G	0.231		
p-G	0.747	p-G	0.075
p-G	0.084	p-G	0.697

electron-electron-nucleus function. They are defined as follows:

$$U_{en}(\bar{\mathbf{r}}) = \sum_i^N \sum_a^M \left[-Z_a \frac{1 - e^{-b_1 \sqrt[4]{2Z_a} r_{ia}}}{b_1 \sqrt[4]{2Z_a}} \right.$$
$$\left. + \sum_{\mu_a} f_{\mu_a}^a \chi_{a,\mu_a}(\mathbf{r}_i) \right], \tag{14}$$

$$U_{ee}(\bar{\mathbf{r}}) = \sum_{i<j}^N \left[\frac{r_{ij}}{2(1 + b_2 r_{ij})} \right], \tag{15}$$

$$U_{een}(\bar{\mathbf{r}}) = \sum_{i<j}^N \sum_a^M \sum_{\mu_a,\nu_a} \left[\bar{f}_{\mu_a,\nu_a}^a \right.$$
$$\left. \chi_{a,\mu_a}(\mathbf{r}_i) \; \chi_{a,\nu_a}(\mathbf{r}_j) \right], \tag{16}$$

where the vector $\mathbf{r}_{ia} = \mathbf{r}_i - \mathbf{R}_a$ is the difference between the position of the nucleus a and the electron i, r_{ia} is the corresponding distance, r_{ij} is the distance between electrons i and j, Z_a is the electronic charge of the nucleus (or pseudo nucleus) a, χ_{a,μ_a} are the atomic orbitals of nucleus a, and b_1, b_2, $f_{\mu_a}^a$, and $\bar{f}_{\mu_a,\nu_a}^a$ are variational parameters. The leading contribution for the description of electronic correlation is given by U_{ee}, but also the inhomogeneous two-electron interaction term U_{een} is important, because they can improve the charge distribution.[60]

At variance of a previous QMC study,[51] in the present VMC-based molecular dynamics, we did not include in the

Jastrow factor the electron-electron-nucleus-nucleus term

$$U_{eenn}(\bar{\mathbf{r}}) = \sum_{i<j}^N \sum_{a \neq b}^M \left[\sum_{\mu_a} \sum_{\mu_b} \tilde{f}_{\mu_a,\mu_b}^{a,b} \chi_{a,\mu_a}(\mathbf{r}_i) \, \chi_{b,\mu_b}(\mathbf{r}_j) \right] \tag{17}$$

that could further improve the description of the long range electron correlation and the charge distribution but require a number of coefficients $f_{\mu_a,\mu_b}^{a,b}$ that grows quadratically with the number of atomic orbitals. Thus, this term is not computationally affordable for a system as large as the ones considered here. On the other hand, the functional form of the homogeneous two-electron interaction term U_{ee} that we are using here has a long-range correlation that satisfactorily recovers a part of the correlation implied by the U_{eenn} term and reproduces the correct bulk properties.

In presence of PBC, the coordinates and the distances are modified in order to fulfill the periodicity of the system, as discussed at the end of Sec. II A. In the Jastrow factor, not only the localized atomic orbitals are modified, but also the homogeneous term in the electron-nucleus and electron-electron terms is obviously affected by this change.

The values of b_1 and b_2 parameters are optimized during the dynamics, and their optimized values are around $\simeq 1$ and $\simeq 0.5$, respectively. We have considered uncontracted atomic orbitals χ_{a,μ_a} of the GTO type for the inhomogeneous terms, and the values of the exponents have been optimized for the water dimer and kept fixed during the VMC-based dynamics, as for the determinant case. The atomic basis set used in this work, including the orbital types and the exponent values for the oxygen and the hydrogen atoms, is specified in Table II.

C. The water dimer as a test case for the wave function ansatz and basis set used in this work

In order to test the reliability of our VMC approach, and, in particular, of the wave function ansatz described in Secs. II A and II B and used for the VMC-based molecular dynamics, we have performed several tests on the water dimer. In the water dimer, the structural minimum, reported in Fig. 1(a), corresponds to a configuration where one water is in the *donor* configuration, and one of its hydrogens (the donor hydrogen H_d) is shared with the other water molecule, the *acceptor* water, forming the *hydrogen bond*. An accurate description of the hydrogen bond is the main ingredient for the description also of the liquid water and of the ice; thus, the water dimer represents a simple meaningful system to check the accuracy of our approach.

The main ingredient for an *ab initio* treatment of the hydrogen bond is the possibility to describe the *dynamical electronic correlation* in the system. This is mainly contained, within our VMC-based approach, in the Jastrow term, whereas the determinantal part of the wave function is more important in the description of strong covalent bonds[54,62–64] and transition states.[65,66] Therefore, we have considered Jastrow terms of increasing size and complexity,[82] and only two different basis sets for the determinantal part of the wave function, that have been indicated by "small-basisX" and "large-basisX," where "X" is a number referring to the size of the Jastrow.
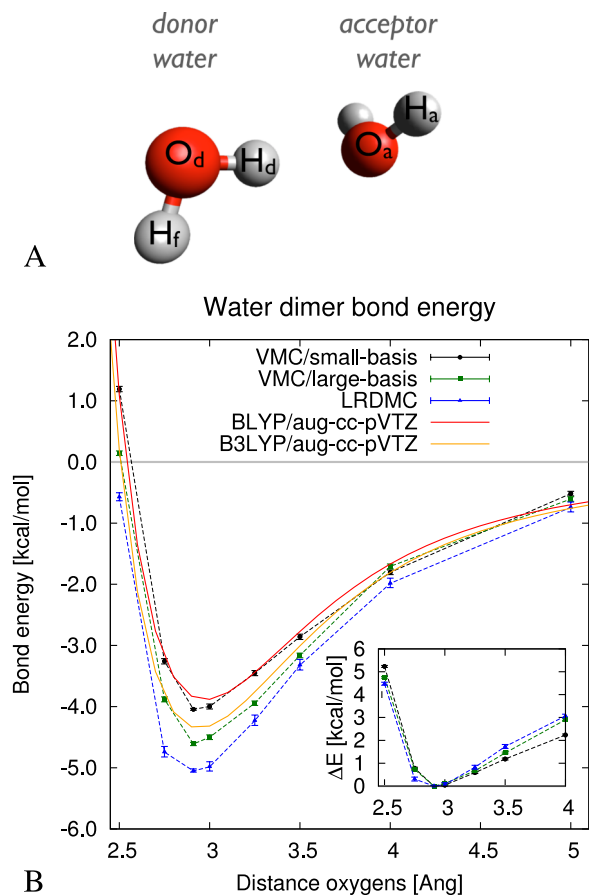
FIG. 1. Panel (a): bonding geometry of the water dimer in its structural minimum. Panel (b): dissociation energy of the water dimer, plotted as a function of the oxygen-oxygen distance, studied with VMC (the small-basis is the one used for the dynamics) and LRDMC (that is almost independent on the choice of the small- or large-basis, see Table IV and Fig. 2). For a comparison, we report also the dissociation curve for DFT/BLYP and DFT/B3LYP, both with aug-cc-pVTZ basis set. Inset: energy difference with the water dimer in its equilibrium configuration. Further details are reported in the text.

The considered basis sets are defined in Table III. In all the reported calculations, the scalar-relativistic energy consistent pseudopotential (ECP) of Burkatzki *et al.*[61] has been adopted in order to describe the two core electrons of the oxygen atoms. We have already shown in Ref. 51 that the use of ECP does not significantly affect the accuracy of the water monomer, as compared with a corresponding all electrons calculation. Moreover, ECP is also particularly convenient as compared with other choices of pseudo-potentials, because it is very favorable from a computational point of view. Notice that the basis that was used for the VMC-based molecular dynamics is the "small-basis1." We also observe that all the bases defined in Table III and here tested have an uncontracted electron-electron-nucleus term U_{een}. This is due to the fact that we have observed that the contraction of the basis, in the U_{een} term, is typically not convenient, because the number of parameters in U_{een} grows only linearly with the size of the basis and of the system, see Eq. (16), and the computational gain with an uncontracted basis is typically important. On the other hand, for the U_{eenn} term, the number of parameters grows quadratically with the size of the basis set and of the system, see Eq. (17); thus, the use of an uncontracted basis turns to be

computationally very expensive and unfeasible for very large systems. We have experienced that the use of hybrid orbitals[51] to contract the orbitals in the U_{eenn} is a very promising strategy, because it allows to minimize the number of parameters without affecting too much the variational flexibility of our Jastrow factor. However, we have chosen for the dynamics a basis without the U_{eenn} term, because the possible improvement in accuracy can be obtained only with further $\simeq 5000$ parameters for a system as large as 32 water molecules. Therefore, in this work, we have finally chosen the simplest basis that guarantees a very stable and efficient optimization during the dynamics.

In Table IV, we report the evaluations of the energy, the variance and the total dipole, obtained for the water monomer and dimer with the different basis sets of Table III. All computations refer to the JSD wave function ansatz and the Jastrow correlated antisymmetrized geminal power (JAGP) ansatz, described in Ref. 59. We have considered both the variational Monte Carlo scheme and the fixed-node lattice regularized diffusion Monte Carlo scheme.[52,53] We evaluate the bonding energy by considering the difference D_e between the energy of the dimer and twice the energy of the monomer, for each wave function ansatz and QMC scheme. For a comparison, in Table IV, we also report the experimental evaluations and the results provided by other computational approaches.

In Table IV, it is shown that, at a variational level, the largest basis sets decrease both the energy and the variance, both for the monomer and the dimer. In particular, the largest variational gains are obtained, in absolute terms, by improving the determinantal part of the wave function: the JSD ansatz with "small-basisX" has a variance of ~0.30 a.u. for the monomer and ~0.59 for the dimer that is reduced, respectively, to ~0.25 and ~0.49 for the JSD ansatz with "large-basisX," and to ~0.21 and ~0.43 for the JAGP ansatz with "large-basisX." However, the improved total energy and variance, obtained by switching from the JSD to the JAGP ansatz, do not necessarily imply an improvement in the H-bond description: for instance, for the large-basis5, the JAGP energy is 5.5 mH lower than the JSD energy for the monomer and 10.3 mH for the dimer, but the evaluation of the H-bond is more accurate for the JSD ansatz (~4.6 mH) rather than for the JAGP ansatz (~4.2 mH). It looks that JAGP is mainly improving the electronic structure of the monomers, but not the H-bond description. Moreover, in the JAGP ansatz, the unphysical charge fluctuations introduced by the AGP part are eliminated only by a very large and, in principle, complete Jastrow term, see Refs. 60 and 73. Therefore, in the JAGP case, the evaluation of the H-bond is affected also by the incomplete description of the Jastrow with a finite basis set. Since the JSD ansatz is not affected by this kind of problem, it is easier to obtain reliable descriptions of the H-bond of the water also with a wave function with a relatively small number of parameters, as the one that we have chosen for the VMC-based dynamics. These considerations have led us to choose the JSD ansatz for the dynamics. Within the JSD ansatz and the VMC scheme, the H-bond evaluation ranges from ~4 kcal/mol for the smallest basis set considered (small-basis1) to ~4.7 kcal/mol for the largest basis sets. In terms of absolute energy, the JSD/large-basis5 leads to a decrease of 2.7 mH in the monomer energy and of 6.3 mH for the dimer energy, with respect to the JSD/small-basis1.

TABLE III. Basis set for water dimer tests. The number of atomic hybrid orbitals is reported in brace parenthesis, whereas "unc." stands for uncontracted orbitals. In the homogeneous electron-nucleus or electron-electron terms of the Jastrow factor, U_{en} and U_{ee}, we indicate with "short" [range] functional form $\frac{1-\exp(-br)}{2b}$, and with "long" [range] functional form $\frac{r}{2(1+br)}$. We use the symbol "=" to indicate that the entry is the same of the previous line. The basis sets are ordered in increasing order of number of variational parameters, thus, of expected accuracy (with the exception of "large-basis4" and "large-basis5" that are equivalent in size). The parameters R_{MAX} indicate the cutoff distance (expressed in atomic units) for the coefficients $g_{\mu_a,\mu_b}^{a,b}$ relative to atoms a and b appearing in the determinantal part of the wave function, as described in Sec. II A; in case the distance $R_{ab} = \|\mathbf{R}_a - \mathbf{R}_b\| > R_{MAX}$, $g_{\mu_a,\mu_b}^{a,b}$ is set to zero and not optimized. Similarly, R_{J-MAX} is the distance cutoff for the $\tilde{f}_{\mu_a,\mu_b}^{a,b}$ coefficients in the electron-electron-nucleus-nucleus term U_{eenn} in the Jastrow factor, see Eq. (17); thus, a value of $R_{J-MAX} = 0$ corresponds to no U_{eenn} term in the Jastrow factor. In the U_{een} and U_{eenn} columns, we indicate the kind of contraction of the orbital functions used for the oxygen and hydrogen atoms. We implicitly assume that these basis sets are used with the scalar-relativistic energy consistent pseudopotential of Burkatzki et al.[61] for the two core electrons of the oxygen atom.

| | Determinant | | | Jastrow | | | | | | |
Name	Oxygen	Hydrogen	R_{MAX}	Oxygen	Hydrogen	U_{een}	U_{eenn}	R_{J-MAX}	U_{en}	U_{ee}
Small-basis1	(5s,5p,1d)/{5}	(3s,1p)/{3}	4.5	(3s,2p)	(2s,2p)	unc.	No	0	Short	Long
Small-basis2	=	=	=	=	=	=	O:{1} H:{1}	∞	=	=
Small-basis3	=	=	=	(3s,2p,1d)	=	=	No	0	=	=
Small-basis4	=	=	=	=	=	=	O:{1} H:{1}	∞	=	=
Small-basis5	=	=	=	=	=	=	unc.	∞	=	=
Large-basis1	(9s,9p,3d,2f)/{12}	(7s,6p,2d)/{4}	∞	(5s,4p,2d,1f)	(3s,2p,1d)	unc.	No	∞	Short	Long
Large-basis2	=	=	=	=	=	=	O:{1} H:{1}	=	=	=
Large-basis3	=	=	=	=	=	=	O:{8} H:{4}	=	=	=
Large-basis4	=	=	=	=	=	=	unc.	=	=	=
Large-basis5	=	=	=	=	=	=	unc.	=	=	Short

In Table IV, we have also reported the results for the LRDMC calculations of the JSD/small-basis1, JSD/large-basis5, and JAGP/large- basis5, and in Fig. 2, we show the dependence on the mesh size a of the total energies and of the binding energy. We observe that the evaluation of D_e is ~5 kcal/mol for all the three wave functions, in agreement with other highly accurate quantum chemical methods such as the couple cluster with single, double, and perturbative triple perturbative excitations (CCSD(T)) or the second order Moller-Plesset (MP2), see Refs. 68 and 70. We also observe that the evaluation of D_e seems not affected by the choice of the LRDMC mesh size a for the JSD ansatz, at least in the range $0.2 \le a \le 0.5$, whereas a small bias with large a can be observed for the JAGP ansatz. Indeed, in Fig. 2, the angular coefficients of the fitting lines for the binding energy are, within the evaluated error of the fitting, compatible with zero for the two JSD calculations, whereas it is not the case for the JAGP wave function. The absolute LRDMC energies for the monomer and the dimer, for the extrapolated $a \to 0$, of the JSD/small-basis1 and JSD/large-basis5 ansatzes differ for less than 0.3 mH, indicating that the small-basis1, although much smaller than the large-basis5 and less accurate at the VMC level, provides a nodal surface that seems as good as the one provided by JSD/large-basis5, because the fixed-node projection scheme yields the same electronic correlation for both wave functions.

The evaluations of the total dipole μ, for the monomer and the dimer show that these quantities are less affected than D_e by the wave function ansatz, and we have obtained reliable values for all the considered methods. In Fig. 3, we have reported a representation of the electronic density for the dimer, calculated with VMC and with LRDMC(a = 0.2). It can be observed that the electrons' distribution is very similar in the two methods. Moreover, we observe that, in the region between the donor hydrogen H_d and the acceptor oxygen O_a,

the electronic density is always larger than 0.02 a.u. (yellow hypersurface in Fig. 3), due to the presence of the H-bond between the two atoms.

The JSD/small-basis1 and JSD/large-basis5 wave functions have also been considered for a structural optimization of the water dimer. The results are reported in Table V and compared with experimental and other *ab initio* computational evaluations. The two wave functions provide structures that are very close, indicating that, at the structural level, the smaller basis does not introduce a large bias, at least at the minimum of the potential energy surface. The main difference between them is in the distance between the oxygens that differs for ~0.02 Å. Anyway, both the results are in good agreement with the experimental evaluations and the reported highly accurate quantum chemical calculations.

In order to check our wave function ansatz not only at the structural minimum but also in a larger region of the potential energy surface (PES), we have considered the dissociation of the water dimer. In Fig. 4, we report the total energy (panel (a)), bond energy (panel (b)), and total dipole (panel (c)) of the water dimer in dissociation. The dissociation is realized by considering structures with increasing oxygen-oxygen distance, $d_{O_d O_a}$, in the dimer. At the PES minimum, the donor hydrogen H_d is rotated of a few degrees from the axis connecting the two oxygens and slightly moved in the direction of the acceptor oxygen O_a with respect to its equilibrium distance in the monomer, see Table V. However, in order to simplify the dissociation plots reported in Fig. 4, we have considered the two water molecules at exactly their equilibrium configuration and relatively oriented in order to have H_d in the oxygens axis, as in Sterpone et al.[74] In Fig. 4(a), we observe that, at the VMC level, each increase in the basis sets, here, considered leads to an improved variational energy, and also the JAGP ansatz provides a large variational improvement when compared with the JSD calculation on the same basis. As expected, the lower

TABLE IV. Energy, variance, and dipole of the water monomer and dimer (respectively, in the experimental and CCSD(T)/cc-pVQZ optimized[67,68] nuclear configuration) evaluated with VMC and LRDMC calculations, with the basis sets and constraints defined in Table III. The bonding energy D_e is evaluated as the difference between the energy of the dimer and twice the energy of the monomer. In the LRDMC calculations, the lattice mesh a is reported in parentheses, with the exception of the $a \to 0$ extrapolation. For a comparison, we also report the values obtained from the experiment and from other computational methods. The stochastic error for the QMC evaluations is reported only for the bonding energy D_e, and it is smaller than 10^{-4} a.u. for the energy evaluations and smaller than 10^{-3} for the variance and dipole evaluations (in the reported units).

| Method | References | Monomer | | | Dimer | | | Bonding[b] D_e |
		E [H]	$VAR(E)$ [H²]	μ (Deb)	E [H]	$VAR(E)$ [H²]	μ (Deb)	(kcal/mol)
VMC/JSD/small-basis1	This work	−17.246 37	0.295	1.886	−34.499 18	0.593	2.563	4.05(4)
VMC/JSD/small-basis2	This work	−17.246 73	0.296	1.887	−34.500 27	0.592	2.559	4.27(6)
VMC/JSD/small-basis3	This work	−17.247 10	0.300	1.891	−34.501 03	0.590	2.554	4.28(6)
VMC/JSD/small-basis4	This work	−17.247 38	0.294	1.888	−34.501 70	0.587	2.559	4.36(7)
VMC/JSD/small-basis5	This work	−17.247 73	0.299	1.890	−34.502 64	0.588	2.555	4.50(8)
VMC/JSD/large-basis1	This work	−17.248 91	0.248	1.919	−34.505 11	0.498	2.566	4.57(5)
VMC/JSD/large-basis2	This work	−17.248 94	0.247	1.855	−34.505 13	0.498	2.520	4.55(5)
VMC/JSD/large-basis3	This work	−17.248 92	0.246	1.853	−34.505 41	0.496	2.520	4.75(5)
VMC/JSD/large-basis4	This work	−17.249 11	0.244	1.895	−34.505 59	0.494	2.545	4.62(5)
VMC/JSD/large-basis5	This work	−17.249 08	0.244	1.882	−34.505 51	0.490	2.544	4.61(5)
VMC/JAGP/large-basis1	This work	−17.254 36	0.215	1.902	−34.514 99	0.438	2.559	3.94(4)
VMC/JAGP/large-basis2	This work	−17.254 42	0.215	1.832	−34.515 24	0.438	2.511	4.01(5)
VMC/JAGP/large-basis3	This work	−17.254 42	0.214	1.835	−34.515 20	0.436	2.503	4.00(10)
VMC/JAGP/large-basis4	This work	−17.254 48	0.213	1.866	−34.515 60	0.430	2.534	4.17(5)
VMC/JAGP/large-basis5	This work	−17.254 61	0.212	1.864	−34.515 86	0.432	2.541	4.17(10)
LRDMC(0.5)/JSD/small-basis1	This work	−17.266 26		1.854	−34.540 73		2.528	5.15(5)
LRDMC(0.4)/JSD/small-basis1	This work	−17.264 88		1.869	−34.537 77		2.546	5.03(5)
LRDMC(0.3)/JSD/small-basis1	This work	−17.263 89		1.877	−34.535 83		2.554	5.06(4)
LRDMC(0.2)/JSD/small-basis1	This work	−17.263 23		1.879	−34.534 52		2.554	5.05(4)
LRDMC/JSD/small-basis1	This work	−17.262 67			−34.533 41			5.06(5)
LRDMC(0.5)/JSD/large-basis5	This work	−17.264 75			−34.537 37			4.94(9)
LRDMC(0.4)/JSD/large-basis5	This work	−17.263 96			−34.535 89			5.00(9)
LRDMC(0.3)/JSD/large-basis5	This work	−17.263 50			−34.535 06			5.06(8)
LRDMC(0.2)/JSD/large-basis5	This work	−17.263 18			−34.534 24			4.94(7)
LRDMC/JSD/large-basis5	This work	−17.262 92			−34.533 74			4.95(10)
LRDMC(0.5)/JAGP/large-basis5	This work	−17.266 83			−34.541 13			4.69(5)
LRDMC(0.4)/JAGP/large-basis5	This work	−17.266 21			−34.540 05			4.78(4)
LRDMC(0.3)/JAGP/large-basis5	This work	−17.265 83			−34.539 38			4.85(5)
LRDMC(0.2)/JAGP/large-basis5	This work	−17.265 50			−34.538 77			4.88(6)
LRDMC/JAGP/large-basis5	This work	−17.265 30			−34.538 39			4.92(7)
BLYP/aug-cc-pVTZ(-f)	69			1.810				4.18
B3LYP/aug-cc-pVTZ(-f)	69			1.856				4.57
CCSD(T)/IO275[a]	70							5.02
CCSD(T)/CBS	68							5.02
MP2/CBS	68							5.03
Experiment	71 and 72			1.855				5.44 ± 0.7[c]

[a]IO275: interaction optimized basis set with 275 basis functions for the H2O dimer., see Ref. 70.

[b]D_e is the total bond energy from the bottom of the well.

[c]The quantity actually measured experimentally is the net bond energy from the lowest vibrational level D_0 that is $D_0 = 3.59 \pm 0.5$ in Ref. 72; D_e was estimated by adding the zero-point energy calculated at the HF/4-21G level.

energy is obtained at the LRDMC level, for which we have considered both the JSD/small-basis1 and the JSD/large-basis5 ansatz. The two different trial wave functions appear to yield to the same energies (once the bias for the finite mesh size a has been evaluated and corrected), within the stochastic errors of the evaluations. In Fig. 4(b), we observe that, at the VMC/JSD level, a larger basis gives essentially a vertical shift of the binding energy, at least for not too large distances. This implies that forces should be quite accurate even for the simplest ansatz

in the mentioned physical range. This is an important property with respect to the molecular dynamics that is sensitive only to the accuracy of forces (slope in the binding) and not to the absolute value of the binding energy. Indeed, at the variational level, it appears difficult to define a Jastrow term with a reasonably small number of parameters that is also able to recover the full dynamical correlation energy, accessible instead at the LRDMC level, providing the correct binding of ~5 kcal/mol. As a further evidence of the quality of our variational approach,
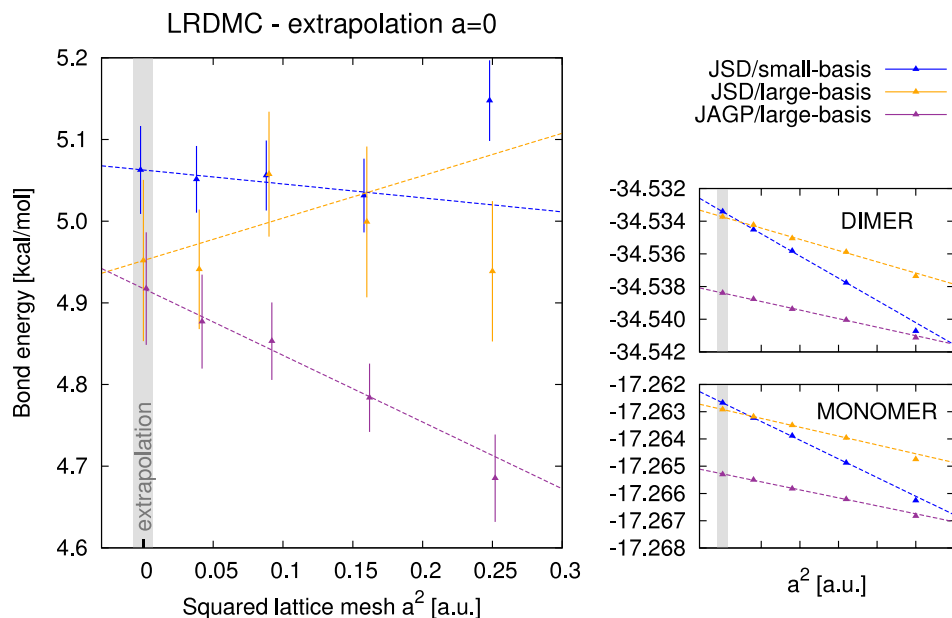
FIG. 2. LRDMC extrapolation of the mesh $a \to 0$, for the total energies of the monomer and of the dimer, and of the binding energy. The corresponding values are also reported in Table IV. The dashed lines correspond to a linear fit of data for the values of the mesh a equal to 0.2, 0.3, and 0.4.

we observe in Fig. 4(c) that the dipole, thus the electronic distribution of the charge, is essentially the same for all the considered methods.

D. Choice of the wave function ansatz

Considering that in the VMC-based molecular dynamics, we need a stable and compact wave function that can be efficiently, quickly, and systematically optimized after every ion movement, and that in the liquid water, every water is surrounded by other four waters, with a distance between the oxygens that may range from ~2.5 Å to ~3.5 Å, we have chosen the smallest considered basis, i.e., JSD/small-basis1. We are confident that the vertical energy shift observed in the water dimer with larger basis sets or ansatzes with a larger number of parameters, see Fig. 4(b), will not affect substantially our results in the liquid water, and that they will be more accurate than the DFT approaches typically used to

FIG. 3. Electronic density of the water dimer, studied with the JSD wave function ansatz and the basis set "small-basis1" (see Table III) which has been used also for the VMC-based molecular dynamics. The upper picture corresponds to a VMC calculations, and the lower picture to a LRDMC calculation with mesh size $a = 0.2$ bohr. The reported hypersurfaces are cut in proximity of the plane defined by the donor water molecule and are colored coded, with white corresponding to a density of 0.01 a.u., yellow to 0.02 a.u., green to 0.04 a.u., cyan to 0.08 a.u., blue to 0.16 a.u., gray to 0.32 a.u., and black to 0.64 a.u.

study the liquid water. Our VMC wave function is, indeed, a real many-body wave function, which recovers the dynamical electronic correlation with the various terms of the Jastrow factor. We have tested it over the water dimer, in Subsection II C, but we think that the improvement of our VMC approach over DFT, in terms of accuracy, is even larger for liquid water, where the packing of the water molecules makes the correlation larger and more challenging. In support of our belief, we show, in Table VI, the dissociation energies of four hexamer clusters of waters, respectively, in prism, cage, book, and ring configurations,[75] calculated with the wave function ansatz and the approach that we have used also for our VMC-based molecular dynamics (VMC with JSD/small-basis1), in comparison with a Hartree-Fock calculation, several DFT calculations with commonly used density functionals, and with some highly accurate quantum chemical approaches: namely, diffusion Monte Carlo (DMC), MP2 perturbation theory, and CCSD(T). In the table, we can observe, in agreement with Refs. 75 and 77, that the typical DFT approaches rank the four hexamers in the wrong way, in relation to their dissociation energy. The VMC calculations obtained with the ansatz used also for the dynamics are instead much more reliable of any of the DFT-based calculations, and they are in fair agreement with the most accurate calculations.

As already observed, the accuracy of QMC-based calculations is further improved and indistinguishable from the best known results if the lattice regularized diffusion Monte Carlo method is applied. However, at present, the computer time required for the simulation by LRDMC of several molecules—like the one presented here—is still out of reach. We have to remark that, when considering geometrical relaxation or dynamics, what is important is not the total energy but the forces between couples of atoms, namely, it is crucial to have accurate energy derivatives of the binding energy profile. As it can be seen in the inset of Fig. 1, by shifting the binding energy curve in order to have the minimum on the x-axis (the shift not affecting its derivative), we obtain a rather good description of the binding shape in the relevant region of R between 2.5 Å and
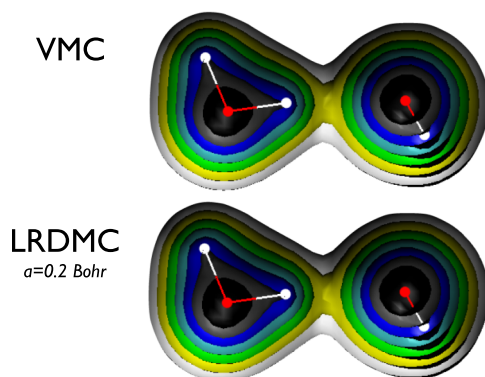
TABLE V. Geometrical properties (Å, deg) for the water dimer, see Fig. 1(a), with the VMC/JSD wave function ansatz used for the VMC-based molecular dynamics, in comparison with the results obtained with VMC/JSD and a larger basis, the experimental values, and results obtained from other computational approaches.

Method	References	$d(O_aO_d)$	$\theta(O_aO_dH_d)$	$d(O_dH_d)$	$d(O_dH_f)$	$d(O_aH_a)$	$\theta(H_dO_dH_f)$	$\theta(H_aO_aH_a)$
BLYP/aug-cc-pVTZ(-f)	69	2.952	5.9	0.981	0.971	0.973	104.8	104.7
B3LYP/aug-cc-pVTZ(-f)	69	2.926	5.8	0.970	0.961	0.963	105.4	105.3
CCSD(T)/IO275[a]	70	2.912	5.5	0.964	0.957	0.958	104.8	104.9
CCSD(T)/cc-pVQZ[b]	67	2.910	4.8	0.964	0.957	0.959	104.3	104.6
VMC/JSD/small-basis1[c]	This work	2.966	3.3	0.960	0.953	0.955	104.8	105.0
VMC/JSD/large-basis5[d]	This work	2.942	4.5	0.961	0.953	0.955	105.0	105.2
Experiment	72	2.976 ± 0.030	6 ± 20					

[a]IO275: interaction optimized basis set with 275 basis functions for the H2O dimer., see Ref. 70.
[b]Structure used in the S22-database.[67,68]
[c]Wave function used for VMC-based MD simulations with 32 and 64 waters in PBC box; see Table II.
[d]See Table III.

3.2 Å and an acceptable error in the large distance region. On the other hand, experience has shown that geometrical properties, namely, the force values around equilibrium distance, are very well determined by the simple variational ansatz in Eq. (1), as it is clearly shown in Subsection II C. The LRDMC usually provides only a substantial correction to the energetics, and therefore, it is not expected to play an important role for static quantities like $g(r)$.

III. RESULTS FOR LIQUID WATER

We apply the molecular dynamics driven by quantum Monte Carlo forces (see Sec. II), introduced recently for the simulation of liquid hydrogen at high pressures.[39] We have employed a simulation of 32 waters in the canonical NVT ensemble at ambient temperature $T = 300$ K and experimental density, thus, in a cubic cell with box side $L = 9.86$ Å and PBC. Since the values of the atomic masses are not affecting the static equilibrium properties, we have set both the hydrogen and the oxygen masses to 1 aru, and we have done about 5000 iterations (that we can estimate to roughly correspond to more than 40 ps of simulation in a standard Newtonian MD simulation), where at each iteration, we optimize about 12 000 variational parameters with 9 steps of efficient energy optimizations based on the so called linear method.[78] We have done several tests[38] confirming that it is possible with this
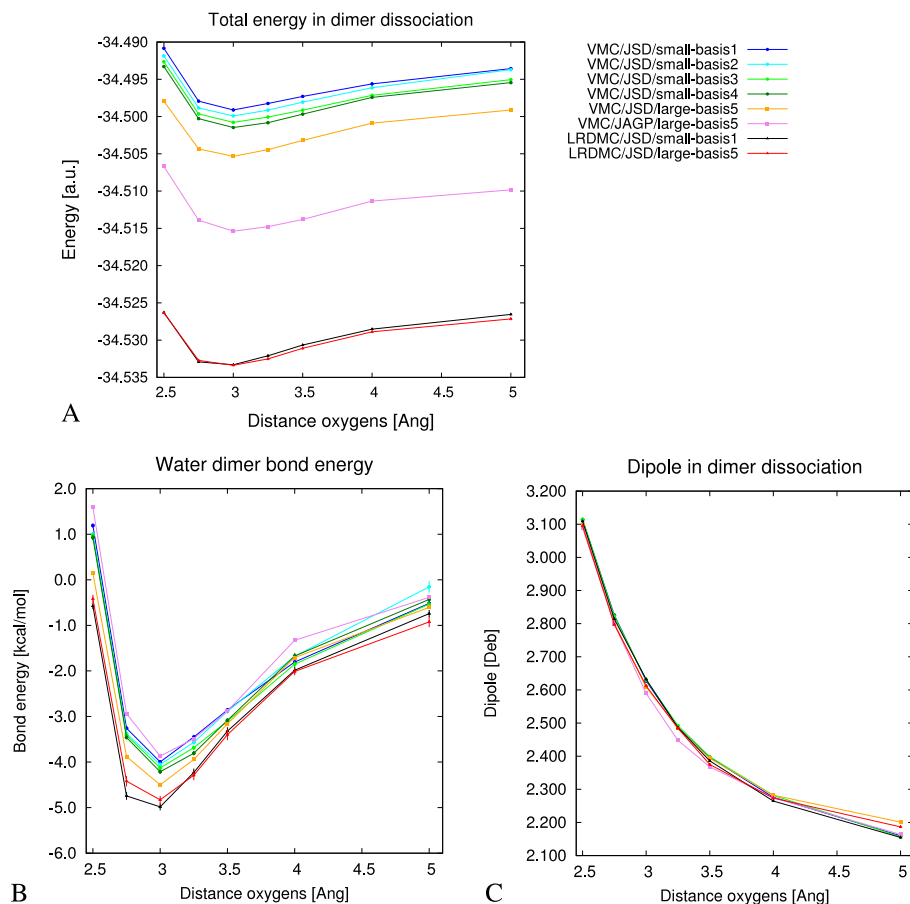

FIG. 4. Total energy (panel (a)), bond energy (panel (b)), and dipole (panel (c)) of the water dimer, plotted as a function of the oxygen-oxygen distance $d_{O_dO_a}$, studied with different VMC ansatzes and basis sets, see text and Table III, using VMC and LRDMC approaches. The LRDMC results are obtained with a mesh size $a = 0.3$ a.u., and the bias due the mesh size has been corrected by assuming that it is the same in all the configurations, so we have used the corrections obtained from Table IV and Fig. 2.

TABLE VI. Dissociation energy of water hexamer clusters, calculated as the energy difference between the energy of the water cluster and six times the energy of the monomer. In parenthesis, it is reported the energy difference between each cluster and the prism cluster. All the values are in mH. The calculations have been done in the geometries optimized with a MP2/aug-cc-pVTZ calculation, taken from Ref. 75. The HF, Local Density Approximation (LDA), PBE, PBE0, BLYP, and B3LYP have been obtained using the Orca package, with an aug-cc-pVTZ basis set. The VMC calculations (in boldface) have been executed with the JSD/small-basis1, as defined in Table III, which has been used also for the VMC-based MD simulation. The stochastic error of the VMC evaluations is of 0.2 mH for the dissociation energy evaluations, and 0.1 mH for the energy difference with the prism cluster. The highly accurate results obtained using DMC, MP2, and CCSD(T) have been taken from the references reported in the table, to with we refer for computational details.

Method		Dissociation energy (mH)			
		Prism	Cage	Book	Ring
HF		−41.7	−41.9(−0.18)	−43.7(−2.04)	−45.7(−3.95)
LDA		−123.3	−123.1(0.17)	−121.7(1.63)	−117.9(5.37)
PBE		−74.8	−75.2(−0.40)	−76.5(−1.70)	−76.0(−1.21)
PBE0		−72.0	−72.3(−0.37)	−73.5(−1.55)	−73.4(−1.42)
BLYP		−60.8	−61.6(−0.76)	−64.0(−3.16)	−64.6(−3.78)
B3LYP		−65.1	−65.7(−0.58)	−67.6(−2.44)	−68.0(−2.87)
VMC/JSD/small-basis1		**−56.9**	**−56.8(0.06)**	**−56.9(−0.09)**	**−55.2(1.67)**
DMC	Reference 75	−73.2	−72.7(0.53)	−72.3(0.90)	−70.7(2.45)
MP2	Reference 75	−73.3	−73.2(0.09)	−72.8(0.46)	−71.5(1.81)
CCSD(T)	Reference 76	−76.6	−76.2(0.46)	−74.7(1.92)	−73.3(3.33)
CCSD(T)	Reference 77		(0.39)	(1.12)	(2.70)

scheme to correctly follow the Born-Oppenheimer energy surface; namely, the variational wave function remains at the minimum possible energy during the time evolution of the atomic positions. The RDFs that we obtain from the VMC-based molecular simulations, having neglected the first 2000 steps of equilibration, are reported in Fig. 5, in comparison with experimental results. We have verified that, within this Langevin scheme, the correlation time estimated by the convergence of the RDF is less than 2000 iterations, and therefore, we are confident that our results represent well equilibrated properties. At variance of the Newtonian dynamics, our advanced method makes use of an appropriate friction matrix, which has been proved to be very helpful to reduce the autocorrelation time[38] as it allows a smooth approach to the equilibrium (see Fig. 6).

As a starting point of our dynamics, we have used equilibrated configurations generated by the DFT molecular dynamics with BLYP functional. The BLYP functional describes the water dimer (the simplest system displaying the hydrogen bond) with a reasonable accuracy, comparable with the one obtained within our VMC scheme, as can be seen in Fig. 1. Nevertheless, the peak positions and shapes of the RDFs are substantially different on the target 32 water system.

We see in Fig. 5 that these first results are very encouraging. Despite the noise, the outcome is quite clear, because the $g_{OO}(r)$ is much closer to experiments than the corresponding DFT calculations. Not only the radial distribution function is much less overstructured but also, as discussed in the Introduction, the position of the first peak is almost indistinguishable from the most recent experiments.[33,34] At this point, it is worth to comment about the error bars in the experimental data. While the Skinner data are extracted from the x-ray scattering intensities, the Soper data[34,35,79] are obtained from Empirical Potential Structural Refinement (EPSR) of joint neutron and x-ray data, i.e., they are not bare neutron diffraction data. The large error bars of Soper (2000) are therefore not directly experimental error bars but they refer to a range of different
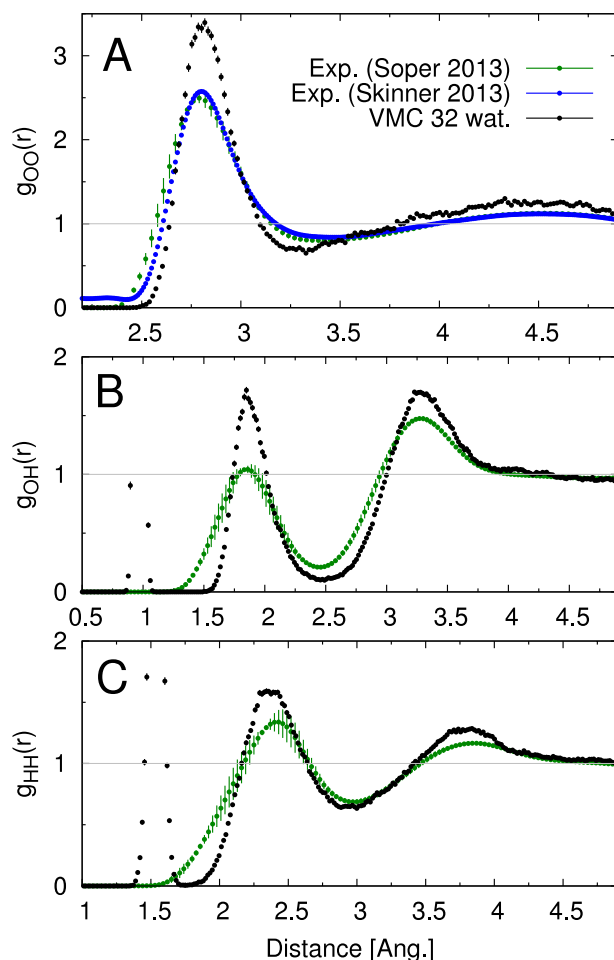

FIG. 5. Radial distribution function obtained with 32 waters by a VMC-based dynamics in NVT ensemble (see text) as compared with the recent X-ray and neutron diffraction experiments of Skinner *et al.*[33] and Soper;[34] panel (a): oxygen-oxygen, panel (b): oxygen-hydrogen, and panel (c): hydrogen-hydrogen. A blow-up of the oxygen-oxygen first peak is reported in Fig. 6.
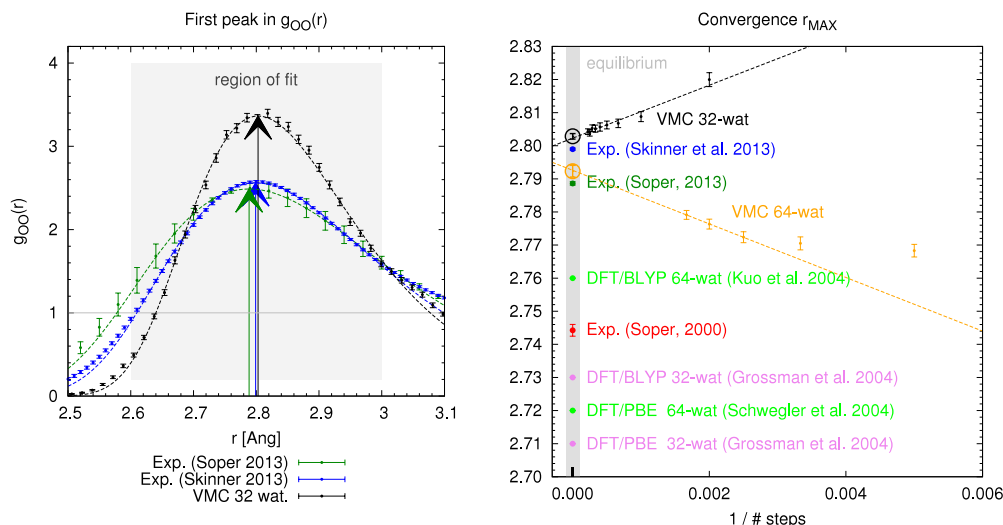
FIG. 6. Left panel: First peak in the oxygen-oxygen radial distribution function obtained from X-ray and neutron diffraction experiments,[33,34] and from the VMC-based MD simulation with a PBC box of 32 waters in NVT ensemble (in black), having neglected the first 2000 steps. The $g_{OO}(r)$ data have been fitted with a Gumbel function in the region of r in the range 2.6–3.0 Å (gray square). The values of r_{MAX} have been highlighted by arrows with corresponding colors. Right panel: r_{MAX} as a function of the inverse VMC-MD simulation length (*i.e.*, the number of steps). The points outside the gray region refer to time averaged quantities obtained without disregarding the initial part of the MD simulation, just to emphasize the smooth approach to equilibrium. Dashed lines interpolating the leftmost points are reported. The equilibrated values, reported inside the gray region, are estimated by eliminating from the trajectory the first part (namely, considering the trajectory from step 2000 to 4500 for the 32 waters, and from 400 to 600 for the 64 waters). The agreement between these values and the linear extrapolations (dashed lines) shows that at least this quantity is equilibrated within the time simulation length. These values are compared with the experimental evaluations and some of the published results[11,12,49] for DFT-based approaches (other results from literature are reported in the Table I).

EPSR fits that would model almost equally well the experimental data. Better fits have been published by the same author more recently, see, e.g., Ref. 34, which reports the likely best structural refinement to date. From the theoretical side, the quality of the approximation used for the electronic correlation affects the accuracy of the RDFs' profile. In fact, the first peak's position has been already improved with respect to standard DFT functionals by employing the simplest (MP2) post-Hatree-Fock technique.[80] Moreover, quantum effects should broaden the peaks without shifting the corresponding maxima, as it was shown before, within DFT, in Ref. 27. Although this remains, until now, a rather controversial issue[32,81] because of the lack of long enough *ab initio* simulations with quantum effects included, our results seem to support the claim made in Ref. 27 about the relevance of proton quantum corrections

in water. Indeed, our RDFs for classical ions remain sizably different from experiments, as far as the broadening and the heights of the first peaks are concerned, especially for what concerns the $g_{OH}(r)$ and $g_{HH}(r)$ radial distribution functions, where quantum effects are expected to be much more important. In addition, quantum effects also enhance the probability of the transient autoprotolysis events, namely, proton transfer between water molecules, which were found in a small but non-negligible fraction by measuring the proton-transfer coordinate.[32] Consistently, during our classical-ions simulation with VMC, the autoprotolysis event has not been observed, see Fig. 7.

In order to avoid possible size effects, we have studied in Fig. 6 the position of the first peak with a much shorter simulation (∼600 steps, corresponding to about 5ps) with 64 molecules. Our method equilibrates rather smoothly with the length of the simulation (say, #steps), and this nice property, coming from our optimized damped MD, has allowed us to obtain a rather well converged value of the peak position also in the 64 water case. This further supports the validity of our claim.

IV. DISCUSSION AND CONCLUSION

In conclusion, we have done the first *ab initio* simulation of liquid water by quantum Monte Carlo, showing that this technique is now mature to enter the field of *ab initio* molecular simulations. This opens a new frontier in water simulations, because several questions about its structure, its electronic properties, and the phase diagram, also difficult to answer experimentally, can be tackled in the near future thanks to the usage of massive parallel supercomputers and quantum Monte Carlo methods. We have adopted the most simple quantum Monte Carlo method (the VMC) in a fully consistent and
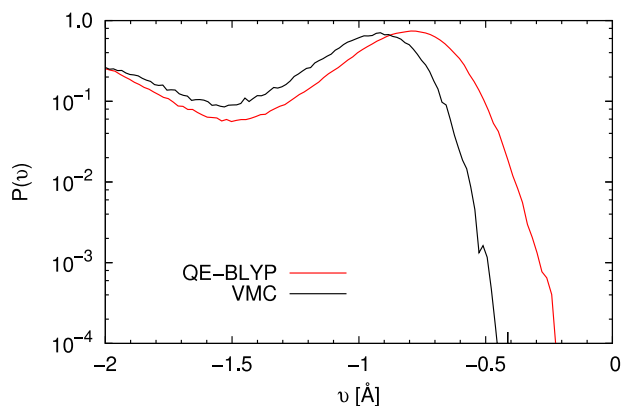

FIG. 7. Distribution of the proton-transfer coordinate in *ab initio* dynamics of liquid water at 300 K. This coordinate is defined as $\nu = d(O_d\text{-}H_d) - d(O_a\text{-}H_d)$ on two water molecules connected by a hydrogen bond (see Fig. 1(a)). We have not observed one event that $\nu > 0$, namely, no transfer among ∼1.8×10^6 and ∼3.6×10^5 hydrogen bonds in BLYP and VMC.

controlled way. Despite the roughness of this first attempt (as compared with the most recent DFT calculations), a few clear results come out from our study.

- The calculation by QMC is feasible albeit computationally heavy, and there is room for considerable improvements along this fully *ab initio* scheme. For instance, it could be possible to work with a larger but more accurate basis (see Fig. 4 and Table IV) with at most a factor ten more computer resources, as our algorithm scales quadratically with the basis dimension. Moreover, even larger improvements in the QMC-based accuracy are expected when moving from the variational scheme, adopted in this work, to fixed-node projection schemes. Fig. 2 shows how both the small and large bases provide a binding energy for the water dimer, evaluated via LRDMC, that is statistically in agreement with highly accurate benchmarks[68,70] coming from CCSD(T) (5.02 kcal/mol). Thus, the most convenient choice is given by the smallest basis, allowing a much cheaper wavefunction optimization during the dynamics and, in principle, also an efficient evaluation of the fixed-node diffusion forces for every new nuclear configuration. However, the DMC is also affected by the finite time step error (in the case of ordinary DMC) or the finite lattice mesh (in the case of the LRDMC scheme used here), and the solution of the infinite variance problem in DMC (or LRDMC) has not been clearly solved yet. Therefore, we expect that the computational cost for this DMC-based molecular dynamics would be easily two order or magnitude larger than the VMC based method proposed here.

- The simulated structural properties of liquid water, obtained within our VMC-based molecular dynamics, appear much closer to the experimental observations when compared with DFT-based molecular dynamics simulations, at least within standard GGA functionals, such as BLYP and PBE. This is remarkable, because, within our approximation, the two-water interaction was basically dealt with the same degree of accuracy of the BLYP functional. As discussed in Subsection II D, this implies that the accurate description of the many water energy surface, and probably the long distance interactions—usually described within DFT by "*ad hoc*" strategies—should be important to close the gap with experiments. In this respect, and in order to support our claim on much simpler systems, we have also verified that our simple variational wave function provides a satisfactory description of water hexamers, in good agreement with the most accurate quantum chemical approaches[75,77]—MP2, DMC, and CCSD(T)—and in contrast with most current DFT functionals for liquid water (see Table VI). In order to put further evidence about the systematic difference between QMC and DFT with BLYP functional, we show in Fig. 8 that the interaction between two water monomers, namely, the repulsive force acting on the O–O axis is much different from the BLYP prediction when they are in the liquid water and not in the vacuum.
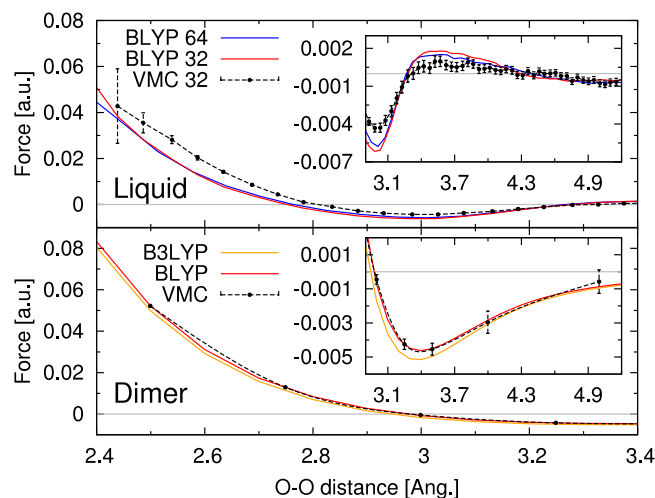

FIG. 8. The net molecular force difference of a pair of water monomers (i, j) projected on their oxygen-oxygen (O–O) direction $(\vec{f}_{H_2O}^{i} - \vec{f}_{H_2O}^{j}) \cdot (\vec{r}_{O_i} - \vec{r}_{O_j})/r_{O_iO_j}$ as a function of O–O distance $r_{O_iO_j}$, where the net molecular force $\vec{f}_{H_2O} = \vec{f}_{H_1} + \vec{f}_{H_2} + \vec{f}_{O}$. The upper panel shows that in liquid water, the VMC and DFT/BLYP forces have sizable difference at short range below 3 Å and the difference between two DFT/BLYP calculations with 32 and 64 molecules in the unit cell is negligible. The lower panel shows that in the water dimer, the two body behavior of VMC, DFT/BLYP, and DFT/B3LYP results is almost the same both at short and long distances.

- It is clear that our work can help the DFT community to define accurate but also consistent functionals, able to reproduce the experimental results, together with a good description of the chemical interactions between water molecules.

- Our agreement with experiment is rather satisfactory and could be probably improved if a larger system (64 waters could be sufficient) and nuclear quantum corrections (not included in this study) would be considered. Indeed, the height of the first peak $g_{OO}^{MAX} = g_{OO}(r_{MAX})$ is expected to be overestimated by ~0.3[5,11] with respect to the converged value in a DFT dynamics with 32 waters. If we assume that also in QMC we have the same effects, the agreement with the experimental value should be substantially improved. Moreover, the inclusion of nuclear quantum effects appears to reduce further the height of the first peak by about ~0.4 (~0.24) if we consider as reference the path integral CPMD calculation reported in Ref. 27 (Ref. 81). Therefore, in future studies, by taking into account both size effects and the effect of quantum nuclei, it may be possible to have a fully consistent *ab initio* description of liquid water by QMC.

We finally remark that, thanks to good scaling properties of QMC algorithms with the system size, this work opens promising perspectives for future applications of such high-level *ab initio* molecular dynamics technique to study the finite temperature properties of complex liquids and materials.

ACKNOWLEDGMENTS

[1]R. Car and M. Parrinello, Phys. Rev. Lett. **55**, 2471 (1985).

[2]K. Laasonen, M. Sprik, M. Parrinello, and R. Car, J. Chem. Phys. **99**, 9080 (1993).

[3]M. Sprik, J. Hutter, and M. Parrinello, J. Chem. Phys. **105**, 1142 (1996).

[4]Z. Ma, Y. Zhang, and M. E. Tuckerman, J. Chem. Phys. **137**, 044506 (2012).

[5]T. D. Kühne, M. Krack, and M. Parrinello, J. Chem. Theory Comput. **5**, 235 (2009).

[6]P. H. L. Sit and N. Marzari, J. Chem. Phys. **122**, 204510 (2005).

[7]S. Yoo, X. C. Zeng, and S. S. Xantheas, J. Chem. Phys. **130**, 221102 (2009).

[8]J. VandeVondele, F. Mohamed, M. Krack, J. Hutter, M. Sprik, and M. Parrinello, J. Chem. Phys. **122**, 014515 (2005).

[9]H.-S. Lee and M. E. Tuckerman, J. Chem. Phys. **125**, 154507 (2006).

[10]H.-S. Lee and M. E. Tuckerman, J. Chem. Phys. **126**, 164501 (2007).

[11]J. C. Grossman, E. Schwegler, E. W. Draeger, F. Gygi, and G. Galli, J. Chem. Phys. **120**, 300 (2004).

[12]I. Kuo, C. Mundy, M. McGrath, J. Siepmann, J. VandeVondele, M. Sprik, J. Hutter, B. Chen, M. Klein, F. Mohamed *et al.*, J. Phys. Chem. B **108**, 12990 (2004).

[13]T. Todorova, A. P. Seitsonen, J. Hutter, I.-F. W. Kuo, and C. J. Mundy, J. Phys. Chem. B **110**, 3685 (2006).

[14]M. Guidon, F. Schiffmann, J. Hutter, and J. VandeVondele, J. Chem. Phys. **128**, 214104 (2008).

[15]C. Zhang, D. Donadio, F. Gygi, and G. Galli, J. Chem. Theory Comput. **7**, 1443 (2011).

[16]R. A. DiStasio, Jr., B. Santra, Z. Li, X. Wu, and R. Car, J. Chem. Phys. **141**, 084502 (2014).

[17]S. Grimme, J. Comput. Chem. **25**, 1463 (2004).

[18]S. Grimme, J. Comput. Chem. **27**, 1787 (2006).

[19]O. von Lilienfeld, I. Tavernelli, U. Rothlisberger, and D. Sebastiani, Phys. Rev. Lett. **93**, 153004 (2004).

[20]M. Dion, H. Rydberg, E. Schröder, D. C. Langreth, and B. I. Lundqvist, Phys. Rev. Lett. **92**, 246401 (2004).

[21]J. Schmidt, J. VandeVondele, I. F. W. Kuo, D. Sebastiani, J. I. Siepmann, J. Hutter, and C. J. Mundy, J. Phys. Chem. B **113**, 11959 (2009).

[22]I.-C. Lin, A. P. Seitsonen, M. D. Coutinho-Neto, I. Tavernelli, and U. Rothlisberger, J. Phys. Chem. B **113**, 1127 (2009).

[23]I.-C. Lin, A. P. Seitsonen, I. Tavernelli, and U. Rothlisberger, J. Chem. Theory Comput. **8**, 3902 (2012).

[24]J. Wang, G. Román-Pérez, J. M. Soler, E. Artacho, and M. V. Fernández-Serra, J. Chem. Phys. **134**, 024516 (2011).

[25]C. Zhang, J. Wu, G. Galli, and F. Gygi, J. Chem. Theory Comput. **7**, 3054 (2011).

[26]M. A. Morales, J. R. Gergely, J. McMinis, J. M. McMahon, J. Kim, and D. M. Ceperley, J. Chem. Theory Comput. **10**, 2355 (2014).

[27]J. Morrone and R. Car, Phys. Rev. Lett. **101**, 017801 (2008).

[28]S. Habershon, T. E. Markland, and D. E. Manolopoulos, J. Chem. Phys. **131**, 024501 (2009).

[29]F. Paesani and G. A. Voth, J. Phys. Chem. B **113**, 5702 (2009).

[30]F. Paesani, S. Yoo, H. J. Bakker, and S. S. Xantheas, J. Phys. Chem. Lett. **1**, 2316 (2010).

[31]X. Z. Li, B. Walker, and A. Michaelides, Proc. Natl. Acad. Sci. U. S. A. **108**, 6369 (2011).

[32]M. Ceriotti, J. Cuny, M. Parrinello, and D. E. Manolopoulos, Proc. Natl. Acad. Sci. U. S. A. **110**, 15591 (2013).

[33]L. B. Skinner, C. Huang, D. Schlesinger, L. G. M. Pettersson, A. Nilsson, and C. J. Benmore, J. Chem. Phys. **138**, 074506 (2013).

[34]A. K. Soper, ISRN Phys. Chem. **2013**, 1 (2013).

[35]A. K. Soper, Chem. Phys. **258**, 121 (2000).

[36]E. Coccia, D. Varsano, and L. Guidoni, J. Chem. Theory Comput. **10**, 501 (2014).

[37]A. Zen, D. Zhelyazov, and L. Guidoni, J. Chem. Theory Comput. **8**, 4204 (2012).

[38]Y. Luo, A. Zen, and S. Sorella, J. Chem. Phys. **141**, 194112 (2014).

[39]G. Mazzola, S. Yunoki, and S. Sorella, Nat. Commun. **5**, 3487 (2014).

[40]G. Mazzola and S. Sorella, Phys. Rev. Lett. **114**, 105701 (2015).

[41]W. M. C. Foulkes, L. Mitas, R. J. Needs, and G. Rajagopal, Rev. Mod. Phys. **73**, 33 (2001).

[42]J. Grossman and L. Mitas, Phys. Rev. Lett. **94**, 056403 (2005).

[43]C. Attaccalite and S. Sorella, Phys. Rev. Lett. **100**, 114501 (2008).

[44]G. Mazzola, A. Zen, and S. Sorella, J. Chem. Phys. **137**, 134112 (2012).

[45]F. A. Reboredo and J. Kim, J. Chem. Phys. **140**, 074103 (2014).

[46]D. M. Ceperley and M. Dewing, J. Chem. Phys. **110**, 9812 (1999).

[47]See s. sorella's talk at the advances in quantum monte carlo techniques for non-relativistic many-body systems http://www.int.washington.edu/talks/WorkShops/int_13_2a/(June 27, 2013).

[48]T. Kühne, M. Krack, F. Mohamed, and M. Parrinello, Phys. Rev. Lett. **98**, 066401 (2007).

[49]E. Schwegler, J. C. Grossman, F. Gygi, and G. Galli, J. Chem. Phys. **121**, 5400 (2004).

[50]N. D. Drummond, M. D. Towler, and R. J. Needs, Phys. Rev. B **70**, 235119 (2004).

[51]A. Zen, Y. Luo, S. Sorella, and L. Guidoni, J. Chem. Theory Comput. **9**, 4332 (2013).

[52]M. Casula, C. Filippi, and S. Sorella, Phys. Rev. Lett. **95**, 100201 (2005).

[53]M. Casula, S. Moroni, S. Sorella, and C. Filippi, J. Chem. Phys. **132**, 154113 (2010).

[54]M. Marchi, S. Azadi, M. Casula, and S. Sorella, J. Chem. Phys. **131**, 154116 (2009).

[55]S. Sorella, *TurboRVB* quantum monte carlo package (accessed date may 2013) URL http://people.sissa.it/~sorella/web/index.html.

[56]C. Attaccalite, Ph.D. thesis, SISSA of Trieste, 2005.

[57]S. Sorella, M. Casula, L. Spanu, and A. Dal Corso, Phys. Rev. B **83**, 075119 (2011).

[58]F. R. Petruzielo, J. Toulouse, and C. J. Umrigar, J. Chem. Phys. **134**, 064104 (2011).

[59]M. Casula and S. Sorella, J. Chem. Phys. **119**, 6500 (2003).

[60]S. Sorella, M. Casula, and D. Rocca, J. Chem. Phys. **127**, 014105 (2007).

[61]M. Burkatzki, C. Filippi, and M. Dolg, J. Chem. Phys. **126**, 234105 (2007).

[62]B. Braïda, J. Toulouse, M. Caffarel, and C. J. Umrigar, J. Chem. Phys. **134**, 084108 (2011).

[63]A. G. Anderson and W. A. Goddard, J. Chem. Phys. **132**, 164110 (2010).

[64]P. M. Zimmerman, J. Toulouse, Z. Zhang, C. B. Musgrave, and C. J. Umrigar, J. Chem. Phys. **131**, 124103 (2009).

[65]A. Zen, E. Coccia, Y. Luo, S. Sorella, and L. Guidoni, J. Chem. Theory Comput. **10**, 1048 (2014).

[66]A. Zen, E. Coccia, S. Gozem, M. Olivucci, and L. Guidoni, J. Chem. Theory Comput. **11**, 992 (2015).

[67]P. Jurecka, J. Sponer, J. Cerny, and P. Hobza, Phys. Chem. Chem. Phys. **8**, 1985 (2006).

[68]S22-benchmark noncovalent complexes, URL http://www.begdb.com/index.php?action=oneDataset&id=4&state=show&order=ASC&by=name_m&method=.

[69]X. Xu and W. A. Goddard, J. Phys. Chem. A **108**, 2305 (2004).

[70]W. Klopper, J. G. C. M van Duijneveldt-van de Rijdt, and F. B. van Duijneveldt, Phys. Chem. Chem. Phys. **2**, 2227 (2000).

[71]S. A. Clough, Y. Beers, G. P. Klein, and L. S. Rothman, J. Chem. Phys. **59**, 2254 (1973).

[72]J. A. Odutola and T. R. Dyke, J. Chem. Phys. **72**, 5062 (1980).

[73]E. Neuscamman, Phys. Rev. Lett. **109**, 203001 (2012).

[74]F. Sterpone, L. Spanu, L. Ferraro, S. Sorella, and L. Guidoni, J. Chem. Theory Comput. **4**, 1428 (2008).

[75]B. Santra, A. Michaelides, M. Fuchs, A. Tkatchenko, C. Filippi, and M. Scheffler, J. Chem. Phys. **129**, 194111 (2008).

[76]R. M. Olson, J. L. Bentz, R. A. Kendall, M. W. Schmidt, and M. S. Gordon, J. Chem. Theory Comput. **3**, 1312 (2007).

[77]M. J. Gillan, F. R. Manby, M. D. Towler, and D. Alfe, J. Chem. Phys. **136**, 244105 (2012).

[78]C. J. Umrigar, J. Toulouse, C. Filippi, S. Sorella, and H. Rhenning, Phys. Rev. Lett **98**, 110201 (2007).

[79]A. Soper and B. C.J., Phys. Rev. Lett. **101**, 065502 (2008).

[80]M. Del Ben, M. Schönherr, J. Hutter, and J. VandeVondele, J. Phys. Chem. Lett. **4**, 3753 (2013).

[81]S. Fritsch, R. Potestio, D. Donadio, and K. Kremer, J. Chem. Theory Comput. **10**, 816 (2014).

[82]We have to remember that in a wave function with a large number of parameters, the variational optimization becomes more challenging and sometimes unstable.